ACS APPLIED ENERGY MATERIALS

www.acsaem.org Article

Li_8ZrO_6 as a Pre-lithiation Additive for Lithium-Ion Batteries

Minog Kim, Brian D. Spindler, Lifeng Dong, and Andreas Stein*

Cite This: *ACS Appl. Energy Mater.* 2022, 5, 14433−14444 Read Online

ACCESS | Metrics & More | Article Recommendations | Supporting Information

ABSTRACT: A major limitation of lithium-ion batteries is that 5−20% of lithium in the cathode is irreversibly lost on the anode surface during the first charge−discharge cycle. This reduces the capacity of the battery for the rest of its operating life. To compensate for the lithium loss, extra lithium can be added to the cathode prior to cell operation, a process called pre-lithiation. Li_8ZrO_6 (LZO) is lithium-rich with 8 Li^+ per formula unit and can potentially provide a large number of lithium ions at relatively low mass loadings to compensate for the irreversible first-cycle capacity loss. LZO was evaluated as a pre-lithiation additive in combination with the cathode material $LiNi_{0.5}Mn_{1.5}O_4$ (LNMO) and assembled in coin cells with graphite as an anode. Two forms of LZO were studied, one synthesized with intrinsic carbon (LZO/C) and one without intrinsic carbon. The fraction of LZO in the composites with LNMO was varied to determine the ratio providing the highest specific capacity per total mass of LNMO and LZO. For the same loading, the LZO additive without intrinsic carbon provided more lithium (5 Li^+ per LZO or 550 mA h/g) than LZO/C (4 Li^+ per LZO or 440 mA h/g) when charged to 4.8 V versus graphite. A loading of 5 wt % LZO was determined to be the optimal amount, delivering the largest number of Li ions with the smallest mass of the LZO additive, which resulted in 10−11% (on the basis of LNMO−LZO mass) or 15−18% (on the basis of LNMO mass) improved reversible specific capacity and 30% improved capacity retention for 50 charge−discharge cycles. Electrochemical impedance spectroscopy revealed that the combined contact and charge transfer resistance of an LNMO half-cell decreases significantly after prelithiation with LZO.

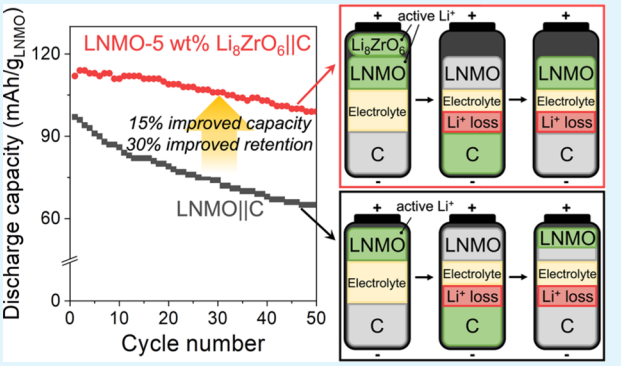

KEYWORDS: *lithium nickel manganese oxide, lithium zirconate, pre-lithiation additive, lithium-ion battery capacity, lithium-rich, electrochemical impedance spectroscopy*

1. INTRODUCTION

Rechargeable lithium-ion batteries (LIBs) are widely used in portable electronic devices, hybrid electric vehicles, and renewable energy storage systems.[1−3] Commercial LIBs typically consist of an intercalation cathode based on a transition metal oxide [such as $LiCoO_2$, $LiMn_2O_4$, $LiNi_{0.5}Mn_{1.5}O_4$ (LNMO), $LiNi_xMn_yCo_zO_2$, and $LiFePO_4$] and a graphite anode.[3,4] When the battery is being charged, Li^+ ions are released from the cathode and incorporated into the anode. During discharge, Li^+ ions are reinserted into the cathode. Unfortunately, during the first charging process, approximately 5−20% of the Li^+ from the cathode is consumed by the formation of a solid electrolyte interphase (SEI) at the anode, resulting in a high irreversible capacity loss and low first-cycle Coulombic efficiency.[5−7]

To mitigate this issue, an extra Li^+ source can be incorporated in the cell to compensate for the first-cycle Li^+ loss. This pre-lithiation additive delivers an excess of Li^+ during the first cycle but becomes inactive during the remaining cycles. The extra Li^+ helps to maintain a higher reversible capacity, prevents the anode from deep cycling, and stabilizes the anode so that capacity retention is improved. Pre-lithiation additives are classified as anode pre-lithiation additives or cathode pre-lithiation additives, depending on their location in the cell.[8−11]

Anode pre-lithiation additives include lithium powder and lithium silicide. Unfortunately, these additives are not compatible with current industrial battery manufacturing processes due to their low potential and high chemical reactivity.[8,12,13] Cathode pre-lithiation additives include sacrificial lithium compounds,[14] conversion-type nanocomposites,[5,6,15] and Li-rich transition metal oxides.[16−19] Sacrificial lithium compounds are moisture-sensitive and release gaseous byproducts while delivering Li^+, which can lead to cracking of the electrode and cause the reversible capacity to decrease.[10,20] Conversion-type nanocomposites, such as metal/Li_2O[5,6] or metal/LiF,[15] require special safety considerations because molten lithium is typically used in their synthesis. Li-rich transition metal oxides, such as Li_2NiO_2 and Li_6CoO_4, are safer

Received: September 14, 2022
Accepted: November 1, 2022
Published: November 14, 2022

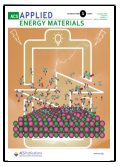

to handle but provide lower specific capacity (<400 mA h/g)[16,19] than other types of cathode pre-lithiation additives.[10] At this point, one of the most promising pre-lithiation agents is Li_5FeO_4, which can deliver ~700 mA h/g (corresponding to 4 Li^+ per formula unit) when charged to 5 V versus Li/Li^+ or ~500 mA h/g (corresponding to 3 Li^+ per formula unit) when charged to 4.8 V versus graphite.[17,18,21] Delithiation of Li_5FeO_4 leaves a stable $LiFeO_2$ residue, which prevents further delithiation.[21] Therefore, there is still a need for new pre-lithiation additives consisting of Li-rich metal oxides with high utilization of Li^+ per unit mass. Here, we are investigating the pseudolamellar metal oxide Li_8ZrO_6 (LZO) as an alternate pre-lithiation source (Figure 1a).

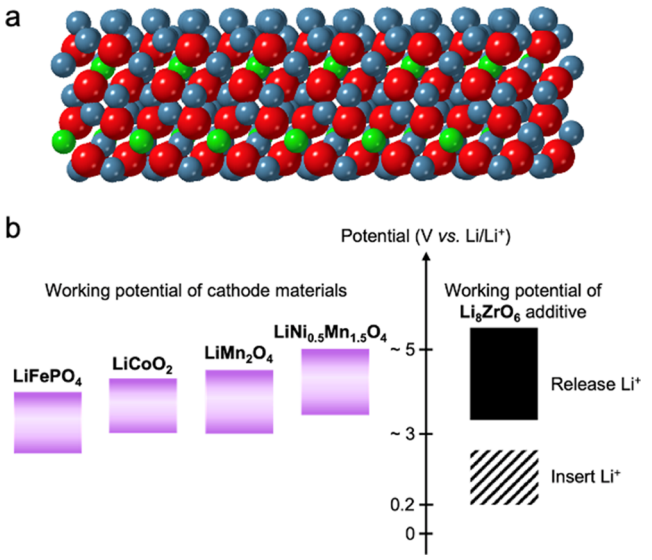

Figure 1. (a) Pseudolamellar structure of LZO. Blue spheres: Li, red spheres: O, and green spheres: Zr. (b) Illustration of the working potential ranges of various cathode materials and LZO. The relatively high working potential range of LNMO most closely matches the potential range during which Li^+ is released from LZO, while not overlapping with the potential range in which Li^+ is reinserted into LZO. The working potential of LZO was obtained from our previous work.[25]

Previously, LZO was studied in our group as a potential cathode material because, with 8 Li^+ per formula unit, it is Li-rich, with each lithium contributing 110.5 mA h/g.[22−25] The effects of doping LZO with transition metals[22−24] or including intrinsic carbon from a precursor component[25] on the performance of LIB half-cells were reported. Half-cells could be reversibly cycled to a depth of 2−3 Li per formula unit.[22−25] Nevertheless, utilization of LZO as a cathode material was limited due to its low electrical conductivity of $(8.6 \pm 2.6) \times 10^{-11}$ S/cm,[24] which resulted in a large hysteresis of the charge−discharge profile. Also, irreversible structural changes were observed during deep charging to remove more than 3 Li per formula unit.[25] While this limits the specific capacity of LZO as a cathode material, irreversible delithiation at deep levels is an attractive feature when considering LZO as a pre-lithiation agent.

Here, we utilized LZO as a pre-lithiation additive instead of a cathode material because we noted that these properties of LZO meet several requirements for a pre-lithiation additive. We hypothesized that, due to its high Li^+ content, only a minimal amount of LZO would be needed to compensate for the irreversible capacity loss in the first charge−discharge cycle. Also, both the synthesis and the utilization of LZO are compatible with existing cell fabrication processes, as demonstrated in our earlier work.[22−25] Moreover, large potential hysteresis resulting from the low electrical conductivity of LZO allows LZO to only release (delithiate) Li^+ while not taking Li^+ back during cell discharge in the operating range of an appropriately chosen cathode material. After releasing Li^+ at deep charge levels (>5 Li/formula unit), the crystalline structure of LZO is irreversibly lost, as confirmed by density functional theory calculations and ex situ X-ray diffraction studies;[25] this would allow LZO used as a pre-lithiation agent to be active only during the first cycle and inactive during subsequent cycles, which is one of the requirements for pre-lithiation additives.

To test our hypothesis, we selected LNMO as the cathode material because its working potential range (3.5−4.9 vs Li/Li^+) would allow LZO to release Li^+ as fully as possible while not taking Li^+ back (Figure 1b). The effects of LZO materials, either with or without intrinsic carbon, were studied in half-cells or full cells with graphite as the anode. Differences in performance of these pre-lithiation additives were interpreted using electrochemical impedance spectroscopy (EIS) data.

2. EXPERIMENTAL SECTION

2.1. Chemicals. Zirconyl chloride octahydrate (98%), zirconium oxynitrate hydrate (99%), and *N*-methyl-2-pyrrolidone (NMP, anhydrous, 99.5%) were purchased from Sigma-Aldrich. Graphite (SLC 1520T) was provided by Superior Graphite. Lithium benzoate (>99%), lithium nitrate (99%), and Li foil (99.9%) were purchased from Alfa Aesar. Copper foil for the battery anode substrate (99.9% Cu, 18 μm thick) was purchased from Online Metals. LNMO (≤100%), aluminum foil for the battery cathode substrate (180 mm width × 15 μm thick), polyvinylidene fluoride (PVDF) (≥99.5%), Super P conductive carbon black, coin cell cases, stainless steel wave springs, and spacers were purchased from MTI Corporation. Celgard 3501 membranes (25 μm microporous monolayer polypropylene) were purchased from Celgard. The battery electrolyte [1.0 M $LiPF_6$ in ethylene carbonate/diethyl carbonate (3:7 wt/wt)] was purchased from Gotion. All gases were purchased from Airgas. All chemicals were used without further purification.

2.2. Synthesis of LZO with Intrinsic Carbon (LZO/C). The synthesis of LZO with intrinsic carbon (LZO/C) was adopted from a previous report.[25] Zirconyl chloride octahydrate (3.1 mmol) and lithium benzoate (37 mmol) were blended by using a zirconia ball-and-cup set in a 8000M mixer/mill (SPEX) in 5 min intervals for a total of 10 min. The as-prepared samples were pyrolyzed under nitrogen (0.6 L/min) in a tube furnace using a thermal gradient of 1 °C/min from room temperature to 600 °C, followed by a 2 h isothermal step, and then heated to 800 °C at 2 °C/min, followed by an additional 2 h isothermal step at 800 °C. The pyrolyzed sample was cooled down to room temperature under nitrogen. The black product contained 33 ± 2 wt % carbon, as determined by combustion-based elemental analysis at Atlantic Microlab, Norcross, GA. This material was denoted as LZO/C. A mixture of this product and Super P conductive carbon black (70:20 wt/wt) was then ball-milled for a total of 30 min in 5 min intervals to homogenize the mixture and reduce the grain size of LZO.[25] This mixture, consisting of 52 wt % LZO and 48 wt % carbon (26 wt % intrinsic carbon and 22 wt % Super P carbon), was used for the preparation of LZO/C electrodes.

2.3. Synthesis of LZO. Carbon-free LZO was synthesized by following our previously published synthetic method.[22] Zirconium oxynitrate (6 mmol) and lithium nitrate (60 mmol) were blended by using a zirconia ball-and-cup set for 5 min. The mixture was calcined in a covered alumina crucible using a thermal gradient of 2 °C/min from room temperature to 600 °C, followed by a 2 h isothermal step

https://doi.org/10.1021/acsaem.2c02980
ACS Appl. Energy Mater. 2022, 5, 14433−14444

Table 1. Summary of Averaged and Highest Capacities (in Parentheses) of LNMO−LZO/C||Graphite and LNMO−LZO|| Graphite Full Cells in the First Cycle (or Highest Capacity Cycle) and Capacity Retention for 50 Cycles

LZO source	amount of the LZO additive in the electrode (wt %)	1st charge capacity[a] (mA h/$g_{LNMO-LZO}$)	Li^+ released per LZO[b]	1st (or highest) discharge capacity[a,c] (mA h/$g_{LNMO-LZO}$)	1st (or highest) discharge capacity[a,c] (mAh/g_{LNMO})	capacity retention for 50 cycles[d] (%)
n/a	0	124 ± 4	n/a	97 ± 5	97 ± 5	66
LZO/C	5	128 ± 3	2	99 ± 3 (102 ± 9)	104 ± 3 (107 ± 10)	79 (77)
	9	151 ± 6	4	99 ± 1 (102 ± 3)	108 ± 1 (112 ± 3)	84 (81)
	13	144	2.5	95 (97)	108 (111)	74 (72)
LZO	5	146 ± 3	5	107 ± 3 (108 ± 2)	112 ± 3 (114 ± 3)	88 (87)
	9	163 ± 3	5	100 ± 3 (106 ± 3)	110 ± 3 (116 ± 3)	83 (78)

[a]Standard deviations, where shown, are based on three cells each. [b]The number of Li^+ supplied from LZO was converted from the specific capacities of LNMO−LZO/C or LNMO−LZO full cells. For example, the increased specific charge capacities provided by LZO at 5 and 9 wt % loadings corresponded to 5 Li^+ out of 8 Li^+ from LZO. This value was calculated as follows: $\frac{146\ \text{mA h/g} - 124\ \text{mA h/g} \times 0.95}{0.05 \times 110.5\ \text{mA h/g}} \cong 5$; $\frac{163\ \text{mA h/g} - 124\ \text{mA h/g} \times 0.91}{0.09 \times 110.5\ \text{mA h/g}} \cong 5$ [c]For LNMO−LZO/C||graphite and LNMO−LZO||graphite full cells, the 1st cycle was used for averaged capacities and the 2nd, 3rd, or 4th cycle in the case of highest capacities, where indicated with parentheses. The specific discharge capacities of the first few cycles were slightly lower than those of a later cycle. This may be attributed to multiple reasons, such as intrinsic reactions induced by irreversible structure changes, kinetic limitations, and parasitic side reactions involving SEI layer formation.[25,37] [d]Capacity retention was calculated by comparing the 1st (or highest) discharge capacity with the 50th cycle discharge capacity (on the basis of LNMO mass).

and then heated to 800 °C at 2 °C /min, followed by an additional 2 h isothermal step at 800 °C. A white powder was obtained by grinding the as-made product using a mortar and pestle. For the preparation of LZO electrodes, this material was ball-milled for a total of 30 min in 5 min intervals using a zirconia ball-and-cup set.

2.4. Preparation of LNMO−LZO/C. Various amounts of LZO/C (containing both intrinsic carbon and Super P carbon) were mixed with LNMO to produce cathodes with different amounts of the pre-lithiation agent. For example, 76 mg of LNMO was mixed with 7 mg of LZO/C, resulting in 5 wt % LZO in the active material (LNMO/LZO = 76:4 wt/wt). This sample was referred to as 5 wt % LNMO−LZO/C. In a similar way, 9 wt % LNMO−LZO/C was prepared by mixing 72 mg of LNMO and 14 mg of LZO/C, and 13 wt % LNMO−LZO/C by mixing 68 mg of LNMO and 20 mg of LZO/C. The 0 wt % sample represents the pristine LNMO without any LZO/C. These wt % values are calculated as fractions of LZO in LMNO with LZO, excluding intrinsic carbon, so that they can be compared more readily with the wt % values for LNMO−LZO without any intrinsic carbon (see below).

2.5. Preparation of LNMO−LZO. As-prepared 30 min ball-milled LZO was mixed with LNMO to achieve a specific fraction of LZO in the active material (LNMO and LZO). For example, 76 mg of LNMO was mixed with 4 mg of LZO to generate 5 wt % of LZO (LNMO/LZO = 76:4 wt/wt) and referred to as 5 wt % LNMO−LZO. A 9 wt % LNMO−LZO sample was prepared by mixing 72 mg of LNMO and 7 mg of LZO. The 0 wt % sample represents the pristine LNMO without any LZO.

2.6. Cell Assembly. For half-cell testing of LZO/C, as-prepared LZO/C samples were mixed with 5 wt % PVDF/NMP binder to achieve a final weight ratio of 47 LZO/43 carbon/10 PVDF. For cells with LNMO cathodes, as-prepared LNMO−LZO/C or LNMO−LZO was mixed with 5 wt % PVDF/NMP binder and appropriate amounts of Super P carbon to achieve a final weight ratio of 80 active material: 10 carbon: 10 PVDF. The amount of active material includes LNMO and the pre-lithiation additive. The carbon includes a mixture of intrinsic carbon and Super P carbon (in the case of using LZO/C) or only Super P carbon (in the case of using LZO). For example, for the 5 wt % LNMO−LZO/C electrode, a mixture of 76 mg LNMO with 7 mg LZO/C (which consists of 4 mg LZO and 3 mg intrinsic carbon) was blended with an additional 7 mg Super P carbon and 10 mg PVDF (obtained from 200 mg of 5 wt % PVDF/NMP binder). For the 5 wt % LNMO−LZO electrode, a mixture of 76 mg LNMO and 4 mg LZO was blended with 10 mg Super P carbon and 10 mg PVDF. For the anode used in full cells, graphite was blended with Super P carbon and the PVDF binder to achieve a final weight ratio of 92:2:6. A slurry was prepared by grinding the mixture using a mortar and pestle. Desirable masses of the slurry were cast onto aluminum foil (for the cathode) or copper foil (for the anode) using a doctor blade (e.g., ∼1 mg/cm^2 of graphite and ∼3 mg/cm^2 of LNMO−LZO). The electrode films were prepared and dried in a dry room (maintaining <100 ppm H_2O). The dried electrode films were pressed using a mechanical roller press, and the electrode was punched out using a 9/16 in. (in diameter) hole punch.

All CR2032 coin cells were assembled in an argon-filled glovebox (<0.1 ppm of H_2O and O_2) using a microporous polypropylene membrane (Celgard 3501) as a separator and 1.0 M $LiPF_6$ in ethylene carbonate/diethyl carbonate (3:7 wt/wt) as the electrolyte. For half-cells, Li foil was used as the anode. For full cells, graphite was used as the anode. The coin cells were sealed using a coin cell crimping machine at a pressure of 750 psi. The sealed coin cells were tested after allowing full infiltration of the electrolyte into the electrode for at least 10 h.

2.7. Structural Characterization. Powder XRD patterns were obtained using an X'Pert Pro diffractometer with an X'Celerator detector and a Co anode (Kα, λ = 1.789 Å) operated at 45 kV and 40 mA. The material morphologies were studied using a JEOL 6500 scanning electron microscope (SEM) operated at a 5.0 kV accelerating voltage after the materials were coated with 50 Å of Pt.

2.8. Electrochemical Measurements. Electrochemical tests were performed using an Arbin BT 2043 test system. For LNMO, there is a possibility that it releases excess Li^+ in the potential range below 3.0 V versus Li/Li^+ (Figure S1).[26−29] This can occur when excess Li is introduced during the synthesis. Usually, an excess of Li is added to compensate for the loss of Li at high synthesis temperatures. A large excess of Li insertion in LNMO leads to a phase transition from a cubic to a tetragonal structure when lithium is added to the octahedral sites of the cubic structure.[28] In this case, the tetragonal phase can be detected in the XRD pattern. If the amount of excess Li is small, it leads to a rock salt impurity, such as $Li_xNi_{1-x}O_2$, Ni_xO or $Li_xNi_yMn_zO_2$, due to oxygen or nickel deficiencies.[30] In our case, the major phase was LNMO with a small amount of a rock salt impurity (Figure S2). If release of excess Li^+ from LNMO occurred, it would be difficult to distinguish it from the effects of a pre-lithiation additive. Therefore, to avoid this situation, the LNMO was preconditioned for five cycles in the narrow potential range from 3.5 to 4.0 V versus Li/Li^+ at 0.05 C (1 C = 147 mA/g LNMO) (Figure S1). This potential range was selected because LZO does not release significant amounts of Li^+ within this range at 0.05 C (1 C = 110.5 mA h/g), as shown in Figure S3. All of the coin cells were preconditioned in this manner. Then, the half-cells were charged and discharged under "normal conditions" for 10 or 50 cycles in the potential range of 3.5 to 4.9 V versus Li/Li^+ at 0.2 C. The specific capacities were calculated by the mass of active materials. For example, for the LZO/C half-cell, it was calculated using the LZO mass but excluding the amount of intrinsic

https://doi.org/10.1021/acsaem.2c02980
ACS Appl. Energy Mater. 2022, 5, 14433−14444

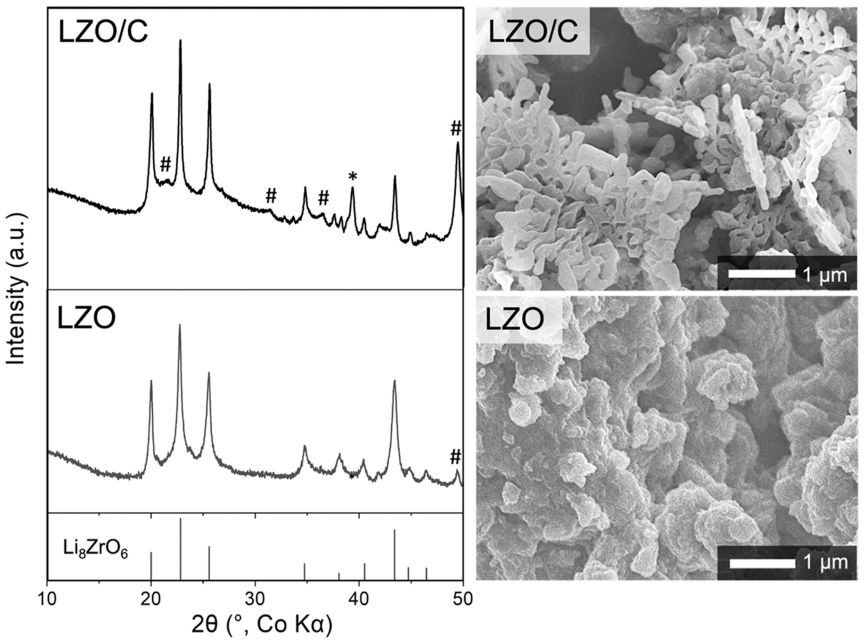

Figure 2. Powder XRD patterns and SEM images of LZO/C and LZO after 30 min of ball-milling. The line pattern was obtained from the International Center for Diffraction Data (ICDD) database, powder diffraction file (PDF) #00-026-0867 (LZO). Reflections marked # are assigned to $Li_6Zr_2O_7$ and * to Li_2O impurity phases.

carbon. For LNMO−LZO/C half-cells and full cells, the specific capacities were calculated based on either LNMO mass or LNMO−LZO mass but excluding the intrinsic carbon. Similarly, for LNMO−LZO half-cells and full cells, the specific capacities were calculated based on either LNMO mass or LNMO−LZO mass, as indicated. The graphite half-cells were cycled in the potential range from 0.01 to 2.0 V versus Li/Li^+ at 0.2 C (1 C = 372 mA h/g graphite).

For full cells, a potential range from 3.4 to 3.9 V at 0.05 C was chosen for the first five preconditioning cycles and a range from 3.4 to 4.8 V at 0.2 C for subsequent cycles. For all cells containing LNMO, cycle 1 refers to the first cycle after preconditioning.

Coulombic efficiency for the cathode was calculated by the following equation

$$\text{Coulombic efficiency (\%)} = \frac{\text{discharge capacity}}{\text{charge capacity}} \times 100\%$$

Coulombic efficiency for the anode was calculated by the following equation

$$\text{Coulombic efficiency (\%)} = \frac{\text{charge capacity}}{\text{discharge capacity}} \times 100\%$$

Capacity retention for 50 cycles was calculated by the following equation

$$\text{Capacity retention (\%)} = \frac{\text{discharge capacity in cycle 50}}{\text{discharge capacity in cycle 1}} \times 100\%$$

If different numbers of cycles were chosen, the numbers of cycles are indicated in the corresponding footnotes for Table 1.

2.9. EIS Experiments. Coin half-cells were assembled for EIS with the following cathode materials. For the LZO/C half-cell, LZO with 33% intrinsic carbon was mixed with the PVDF binder to achieve a weight ratio of 60 LZO/30 intrinsic carbon/10 PVDF. For the LZO half-cell, pure LZO was mixed with Super P carbon and PVDF binder to achieve a weight ratio of 60 LZO/30 Super P carbon/10 PVDF. Cells containing LNMO−LZO/C and LNMO−LZO were prepared in the same way as described above in Section 2.6. All half-cells were preconditioned for five cycles in the narrow potential range of 3.5 to 4.0 V versus Li/Li^+ at 0.05 C (1 C = 110.5 mA/g LZO).

Impedance spectra were collected using a Solartron SI1287 electrochemical interface with a SI1255B frequency response analyzer and applying a sinusoidal perturbation with a 10 mV amplitude from 1 MHz to 10 mHz. 10 points per decade frequency were collected. The impedance spectra were fit using Zview software from Scribner Associates Inc. To avoid fitting artifacts at high frequencies, fitting was performed in the range of 20 kHz to 10 mHz. LZO half-cells were fit using the equivalent circuit shown in Figure S4 and LZO/C half-cells as well as half-cells with LNMO and various amounts of LZO or LZO/C were fit using the equivalent circuit shown in Figure S5.

3. RESULTS AND DISCUSSION

3.1. Preparation of the Pre-lithiation Additives and Cathode Materials. LZO was incorporated into LNMO cathode materials as a pre-lithiation additive in two different forms, one containing intrinsic carbon from one of the precursors (denoted as LZO/C) and the other lacking any intrinsic carbon (denoted as LZO). The former material contained 33 wt % intrinsic carbon generated during the thermal decomposition of the lithium benzoate precursor used in the solid-state synthesis of LZO. This intrinsic carbon was previously shown to improve the electrical conductivity of LZO when used as an LIB cathode material.[25] The SEM image of LZO/C shows a relatively open, coral-like structure of nanoparticle aggregates (Figure 2). Its XRD pattern shows reflections from the major LZO phase, as well as peaks from minor impurities of $Li_6Zr_2O_7$ and Li_2O and a broad background peak centered around 30° 2θ due to the intrinsic carbon (Figure 2). Based on our previous work, $Li_6Zr_2O_7$ can be delithiated and relithiated similarly to LZO, whereas Li_2O acts as a highly resistive phase.[25] The average grain size of LZO in LZO/C ball-milled for 30 min was >100 nm, estimated by the Scherrer equation from the full-width-at-half-maximum of the (101) peak at 22.8° 2θ after correction for instrumental broadening. Smaller grain sizes could be obtained by additional ball-milling, but ball-milling times longer than 30 min were avoided to minimize contact with carbon dioxide from the air,

https://doi.org/10.1021/acsaem.2c02980
ACS Appl. Energy Mater. 2022, 5, 14433−14444

which would result in the formation of Li_2CO_3 as an inactive impurity phase.[31]

The other form of the pre-lithiation additive, LZO, was synthesized with lithium nitrate as the lithium precursor and did not contain any intrinsic carbon.[22] This sample was also ball-milled for 30 min to reduce the grain size. The average grain size of LZO decreased from >100 to 60 nm after 30 min of ball-milling (Figure S6). Based on its XRD pattern, LZO consists mainly of the LZO phase with only very small peaks from minor $Li_6Zr_2O_7$ and Li_2O impurity phases. As seen in the SEM image (Figure 2), LZO consisted of denser agglomerates of stacked platelets. Interestingly, the characteristic size of LZO particles was larger than that of individual LZO/C particles, even though the grain size within LZO particles was smaller after the same duration of ball-milling.

For the preparation of the final pre-lithiation additive, in order to increase the conductivity of LZO/C, it was ball-milled together with highly conductive Super P carbon black in LZO/C cells, resulting in a composition of 52 wt % LZO and 48 wt % total carbon (26 wt % intrinsic carbon and 22 wt % Super P carbon). LNMO−LZO/C samples were prepared by blending LNMO and LZO/C to achieve various loadings of LZO in the composite, namely 0, 9, 14, and 27 wt % LZO. Figure S7 shows that LZO peaks started to appear for 9 wt % LZO/C and became more intense with loadings of 14 and 27 wt % LZO, as expected. Similarly, LNMO−LZO cathode materials were prepared with 5, 9, and 27 wt % LZO. Because of the smaller grain size determined for ball-milled LZO and the associated line broadening, reflections from LZO in the XRD patterns of LNMO−LZO blends were very weak, even at a loading as high as 27 wt % (Figure S7).

3.2. Deep Charging of LZO/C in Half-Cells. The electrochemical behavior of LZO/C was studied in coin half-cells to determine the number of lithium ions per formula unit of LZO that could be extracted below 4.9 V versus Li/Li^+. As observed in our previous research,[25] when LZO is delithiated by more than 3 Li^+ per formula unit, it begins to lose its structure and rapidly loses capacity after the first charge−discharge cycle. As an example, Figure 3 shows that with an upper voltage limit of 4.9 V versus Li/Li^+, the specific charge capacity was 545 mA h/g, corresponding to ∼5 Li^+ per formula unit, and the specific discharge capacity was 5 mA h/g for the first cycle. In the second cycle, the specific charge capacity dramatically decreased to 38 mA h/g and kept decreasing to 6 mA h/g by the 10th cycle. The specific discharge capacities remained lower than 5 mA h/g after 10 cycles. Therefore, after deep charge, LZO is only active during the first charge cycle and becomes inactive in subsequent cycles. This behavior of LZO/C indicates promise for use as a pre-lithiation additive within the working voltage range of 3.5−4.9 V versus Li/Li^+, a range that is aligned with the working voltage range of LNMO (Figure 1b). Even deeper charging than 5 Li^+ per formula unit is possible[25] but would require a higher charging voltage than 4.9 V and a high-voltage electrolyte that does not decompose under these conditions.

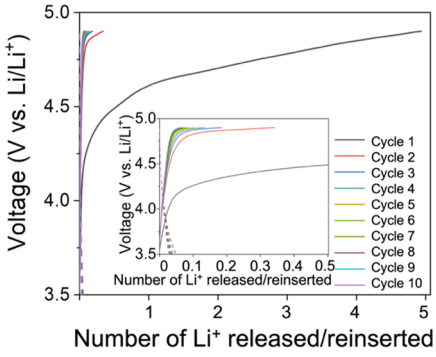

Figure 3. Voltage profiles of a LZO/C half-cell for 10 cycles. The solid lines represent the number of Li^+ released from LZO/C during charge cycles, and the dashed lines represent the number of Li^+ reinserted into LZO/C during discharge cycles. The inset shows an expanded view for the 0−0.5 Li^+ range. The number of Li^+ was calculated using a specific capacity of 110.5 mA h/g for each Li^+ in LZO.

3.3. Electrochemical Behavior of LNMO−LZO/C and LNMO−LZO in Half-Cells. LNMO−LZO/C samples were prepared with various amounts of LZO (from 0 to 18 wt %) in order to study the electrochemical impact of the LZO pre-lithiation additive used in combination with LNMO. Figure 4a,b shows the first cycle voltage profiles of the LNMO−LZO/C cathodes in half-cells. Since LZO is only active during the first charging step, the specific capacity was calculated in two different ways. The specific capacities in Figure 4a were calculated on the basis of the mass of LNMO, whereas those in Figure 4b were calculated on the basis of the combined mass of LNMO and LZO. Pristine LNMO showed the typical high-voltage plateau at ∼4.7 V that is attributed to the $Ni^{2+}/Ni^{3+}/Ni^{4+}$ redox states and another small step at ∼4.0 V that is attributed to the Mn^{3+}/Mn^{4+} redox couple. As the amount of LZO in the LNMO−LZO/C samples was increased, the specific charge capacity also increased until the LZO amount reached 9 wt %; it then decreased for the 18 wt % sample. The decrease at higher LZO loadings is likely due to the low electrical conductivity of LZO.[24,25] As more LZO is incorporated in the cathode, the overall electrical conductivity of the cathode decreases, which results in lower charge capacities. In terms of specific discharge capacities based on the mass of LNMO, the 0−9 wt % LNMO−LZO/C samples maintained approximately the same discharge capacities of 120 mA h/g. This shows that LZO loadings ≤9 wt % did not introduce any detrimental effects to the cathodes. An LZO loading of 13 wt % resulted in a slightly lower discharge capacity of 110 mA h/g, and the discharge capacity with a loading of 18 wt % dropped dramatically to 66 mA h/g due to the low electrical conductivity of LZO. The specific discharge capacities calculated on the basis of the combined mass of LNMO and LZO were slightly lower because the deeply charged LZO was no longer active during the discharge cycle. Figure S8 shows that all of the cells exhibited similar electrochemical behavior after the first charging step regardless of LZO loading because the excess Li^+ from the LZO pre-lithiation additive was only released during the first cycle charging step.

We hypothesized that if additional conductive carbon was introduced to the 18 wt % LNMO−LZO/C material to compensate for the greater electrode resistance at high LZO/C loadings, the specific discharge capacity would be improved. Figure S9 shows that the specific discharge capacity was indeed greatly improved for the 18 wt % LNMO−LZO/C with additional battery-grade Super P carbon. This implied that the intrinsic carbon in the LZO/C was less effective than the battery-grade Super P carbon since the conductivity of carbon depends on multiple parameters, including its structure and degree of graphitization.[32] Therefore, replacement of intrinsic

https://doi.org/10.1021/acsaem.2c02980
ACS Appl. Energy Mater. 2022, 5, 14433−14444

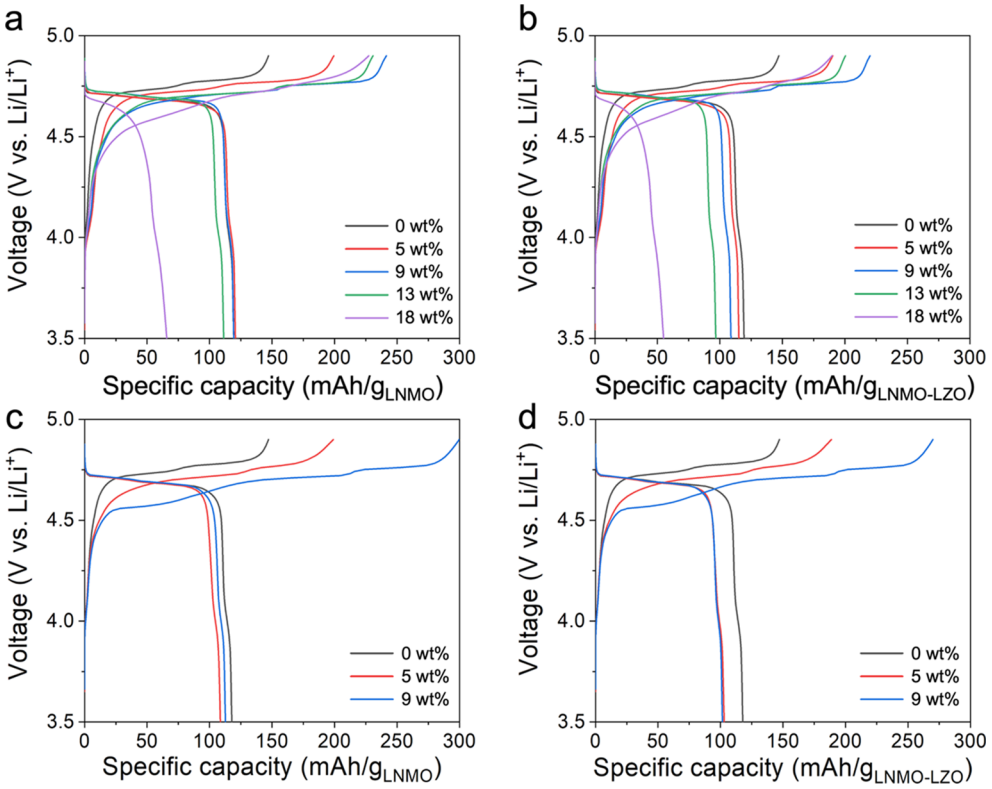

Figure 4. Voltage profiles of (a,b) LNMO−LZO/C half-cells and (c,d) LNMO−LZO half-cells with various loadings of LZO during the first cycle: (a,c) specific capacities calculated on the basis of the mass of LNMO only, and (b,d) specific capacities calculated on the basis of the combined mass of LNMO and LZO.

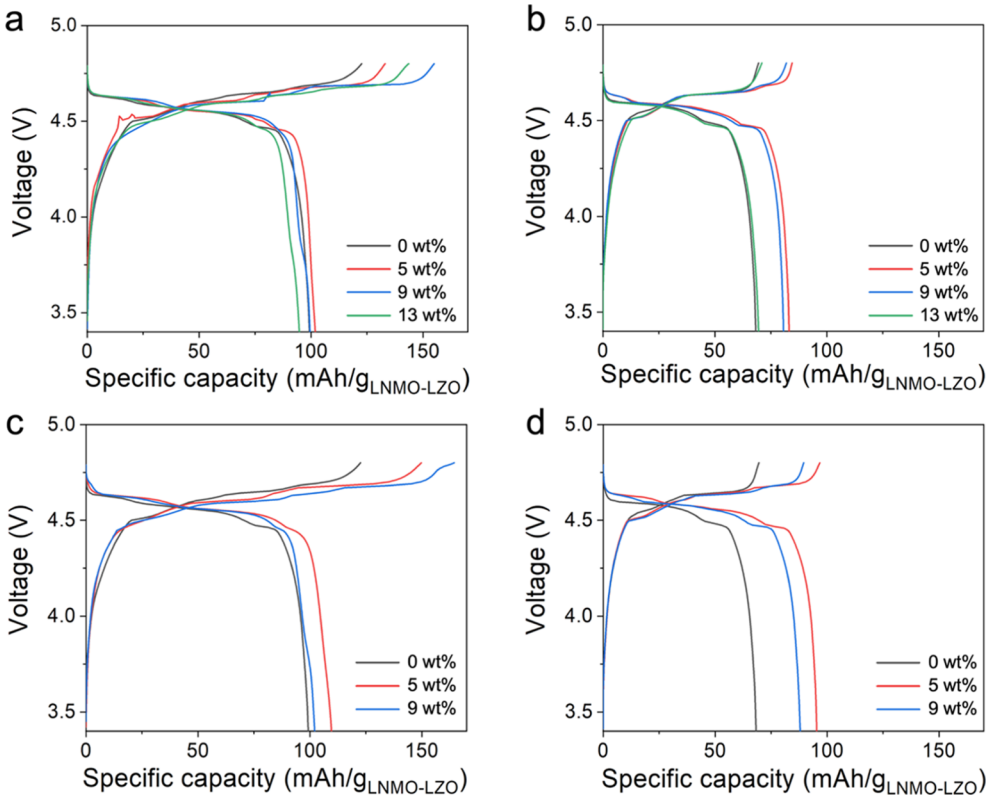

Figure 5. Voltage profiles of (a,b) LNMO−LZO/C||graphite cells and (c,d) LNMO−LZO||graphite cells with various loadings of LZO during (a,c) the first cycle and (b,d) the 50th cycle. Specific capacities were calculated on the basis of the combined mass of LNMO and LZO.

https://doi.org/10.1021/acsaem.2c02980
ACS Appl. Energy Mater. 2022, 5, 14433−14444

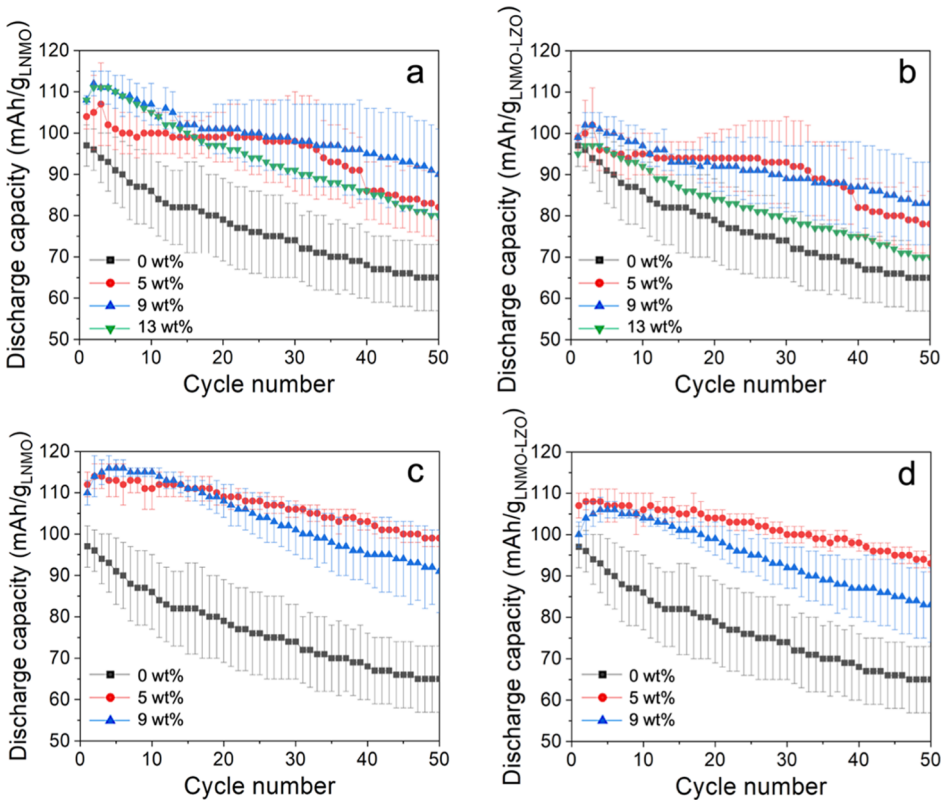

Figure 6. Cycle performance comparison of averaged discharge capacities of (a,b) LNMO−LZO/C||graphite cells and (c,d) LNMO−LZO||graphite cells with various loadings of LZO throughout 50 cycles: (a,c) specific capacities based on the mass of LNMO, and (b,d) specific capacities based on the combined mass of LNMO and LZO. N = 3 for each material except the 13 wt % LNMO−LZO/C||graphite sample because this material was expected to show a lower capacity due to its lower discharge capacity observed in the half-cell tests (Figure 4) and the full cell results shown in Figure 5 and Table 1.

carbon with battery-grade Super P carbon was examined with the goal to further increase achievable capacities.

LNMO−LZO cathodes were prepared with various loadings of LZO to determine the impact of the LZO additive on the LNMO cathode when intrinsic carbon was replaced with Super P carbon. Based on the results of the LNMO−LZO/C half-cell studies, the amount of LZO was chosen to be between 0 and 9 wt %. The first cycle voltage profiles of the LNMO−LZO half-cells are shown in Figure 4c,d. As the LZO loading was increased, the specific charge capacities also increased because of the increased amount of Li^+ available to be released, while the discharge capacities remained similar. This implies that a loading of up to 9 wt % of LZO does not induce any detrimental effects to the cathode electrodes. If the specific capacities are calculated on the basis of the combined mass of LNMO and LZO, the discharge capacities decrease slightly because the LZO is no longer active during the discharge cycles. Judging from the half-cell results of the LNMO−LZO cathodes compared to the LNMO−LZO/C cathodes, more Li^+ would be available for delithiation during the charge process in the former materials. It was difficult to calculate the exact amount of Li^+ due to the possible involvement of electrolyte decomposition in the high voltage range.[20,33,34] Therefore, we did not quantify the number of Li^+ for the half-cells. However, the effect of LZO could be evaluated by studying the charge capacities in full cells that did not have a large reservoir with excess Li^+ in the anode, unlike the half-cells with Li metal.

3.4. Electrochemical Behavior of LNMO−LZO/C and LNMO−LZO in Full Cells. For the full cells, the capacity ratio of the negative electrode to the positive electrode (N/P ratio) was chosen to be close to 1.1 to avoid Li plating on the anode.[35,36] The charge and discharge profile for graphite as the negative electrode is shown in Figure S10. The discharge and charge capacities were 356 and 304 mA h/g, corresponding to an initial Coulombic efficiency of 85%.

The effect of LZO/C as the pre-lithiation additive was examined using LNMO−LZO/C||graphite full cells with varying amounts of LZO/C, ranging from 0 wt % (pristine LNMO) to 13 wt %. Higher loadings were not examined in the full cells because the half-cell experiments had revealed a decrease in electrochemical performance for higher LZO content. Figure 5a,b shows the first cycle and the 50th cycle voltage profiles, and Table 1 summarizes the specific capacities and capacity retention. All of the LNMO−LZO/C||graphite full cells showed a significant improvement in specific charge capacity compared to LNMO||graphite full cells. For LZO/C prelithiation additives with intrinsic carbon, the 9 wt % LNMO−LZO/C||graphite cells showed the highest specific charge capacity compared to LNMO||graphite cells (corresponding to 4 Li provided by LZO per formula unit), followed by 13 wt % LNMO−LZO/C||graphite (2.5 Li/f.u.) and 5 wt % LNMO−LZO/C||graphite (2 Li/f.u.) during the first cycle. The higher charge capacities of the LNMO−LZO/C||graphite full cells resulted from more extensive delithiation of the cathode electrode to compensate for the irreversible capacity loss during the first cycle. As a result, the specific discharge

https://doi.org/10.1021/acsaem.2c02980
ACS Appl. Energy Mater. 2022, 5, 14433−14444

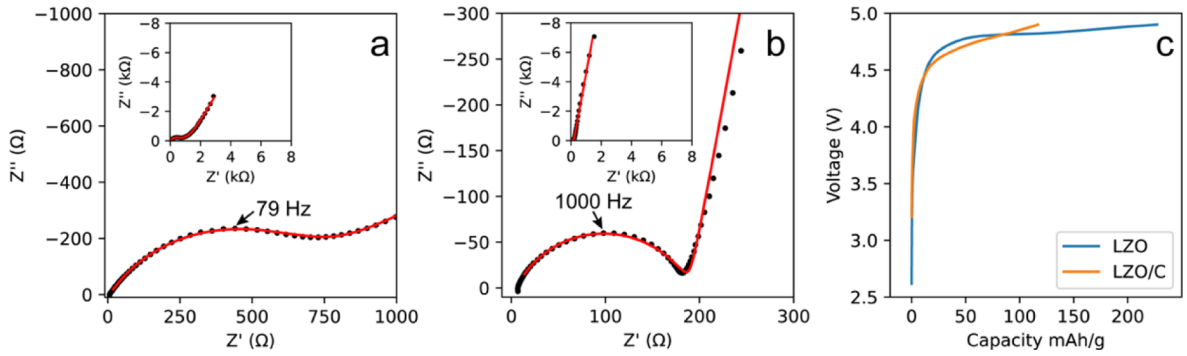

Figure 7. Nyquist plots for (a) LZO/C and (b) LZO half-cells after pre-conditioning. The black dots are the individual data points, and the red line is the fit. (c) Voltage profiles of LZO and LZO/C half-cells during the first charging step after preconditioning, with an upper potential limit of 4.9 V vs Li/Li$^+$ at 0.2 C.

Table 2. Impedance Parameters of Pre-conditioned LZO and LZO/C Half-Cells Obtained from Fitting the EIS Spectra in Figure 7 Using the Equivalent Circuit in Figure S4 for the LZO Half-Cell and the Equivalent Circuit in Figure S5 for the LZO/C Half-Cell[a]

half-cell	R_s (Ω)	R_1 (Ω)	R_2 (Ω)	Q_1 (μF $s^{\alpha-1}$)	Q_2 (μF $s^{\alpha-1}$)	Q_3 (μF $s^{\alpha-1}$)	α_1	α_2	α_3
LZO	4.8 ± 2.0	330 ± 120		11 ± 2		1500 ± 500	0.78 ± 0.03		0.87 ± 0.02
LZO/C	4.4 ± 1.6	810 ± 210	420 ± 100	25 ± 11	220 ± 170	970 ± 490	0.61 ± 0.03	1.0	0.63 ± 0.03

[a]Data is reported as average ± one standard deviation for four replicate cells each. R_s is the solution resistance. R_1 is the contact resistance between the current collector and the active material and may include CEI resistance. R_2 is a combination of pore resistance and charge transfer resistance of the LZO/C. Q_1 is the double-layer capacitance in parallel with the contact resistance. Q_2 is the double-layer capacitance at the LZO/C/electrolyte interface. Q_3 is related to mass transport within the LZO particles.

capacity and capacity retention also improved. The specific discharge capacity increased from 97 mA h/g_{LNMO} for a LNMO||graphite full cell to 108 mA h/g_{LNMO} for a 9 wt % LNMO−LZO/C||graphite full cell, an 11% improvement in the discharge capacity. Although the improvement became smaller when the specific capacity was calculated based on the combined mass of LNMO and LZO, the extra Li$^+$ from the additional LZO in the cathode still helped to prevent graphite from deep cycling, and hence the capacity retention was improved. For example, the 9 wt % LNMO−LZO/C||graphite cell showed a 25% improvement in capacity retention (Figure 6).

The performance of full cells improved further when LZO was used as the pre-lithiation additive instead of LZO/C (Figure 5c,d and Table 1). During the first cycle, the 9 wt % LNMO−LZO||graphite cell showed the highest specific charge capacity increase compared to LNMO||graphite, followed by the 5 wt % LNMO−LZO||graphite cell. However, in terms of specific discharge capacity, the 5 wt % LZO additive showed the greatest improvement compared to the pristine LNMO (10%, from 97 mA h/g_{LNMO} to 107 mA h/$g_{LNMO-LZO}$ on the basis of combined LNMO and LZO mass; 15%, from 97 to 112 mA h/g_{LNMO} on the basis of LNMO mass only). This allowed us to keep the additive amount small in the full cells to maximize the capacity of the active material. The 9 wt % LZO additive resulted in a 13% improvement on the basis of LNMO mass but only in a 3% improved discharge capacity on the basis of combined LNMO and LZO mass due to the increased mass fraction of inactive LZO.

Figure 6c,d shows discharge capacities of LNMO−LZO|| graphite full cells with various amounts of LZO throughout 50 cycles. A clear improvement in capacity retention for 50 cycles was observed with LZO as a pre-lithiation additive (Table 1 and Figure S12). During the 50th cycle, a typical pristine LNMO||graphite full cell showed a significant capacity drop to 70 mA h/g, whereas the 5 wt % LNMO−LZO||graphite cell maintained a specific capacity of 95 mA h/$g_{LNMO-LZO}$ (or 101 mA h/g_{LNMO}), and the 9 wt % LNMO−LZO||graphite cell maintained 88 mA h/$g_{LNMO-LZO}$ (or 97 mA h/g_{LNMO}). With 5 wt % LZO present in the cathode, the capacity retention was 86−87%; in contrast, the cell without LZO retained only 66% of capacity after 50 cycles. Based on these observations, 5 wt % LZO was determined to be the optimal amount of the pre-lithiation additive in combination with LNMO as it delivered the largest number of Li$^+$ ions with the smallest amount of the LZO additive.

Under the conditions studied here, LZO provided approximately 5 Li$^+$ per formula unit when used in combination with the high-voltage cathode material LNMO. As shown in Table S1, the LZO additive also provided a meaningful increase in reversible capacity and capacity retention at relatively low additive amounts when compared with the performance of other representative Li-rich pre-lithiation additives for cathode materials, such as Li_5FeO_4 and Li_6CoO_4.

3.5. Why Does LZO Provide More Capacity Than LZO/C? The question remains why LZO/C with intrinsic carbon was an inferior pre-lithiation agent compared to LZO with an equivalent amount of battery-grade carbon, even though LZO/C performed better as an LIB cathode in previous studies.[25] An analysis of EIS data and SEM images shed some light on this matter.

Figure 7 shows Nyquist plots for pre-conditioned half-cells containing either LZO/C or LZO as the cathode, and Table 2 lists the corresponding impedance parameters. The impedance spectrum of the LZO cell shows a semi-circle that is likely associated with overlapping contributions from electronic contact resistance at the cathode/current collector interface, a surface film resistance associated with the cathode electrolyte interface (CEI), and charge-transfer resistance at the LZO

https://doi.org/10.1021/acsaem.2c02980
ACS Appl. Energy Mater. 2022, 5, 14433−14444

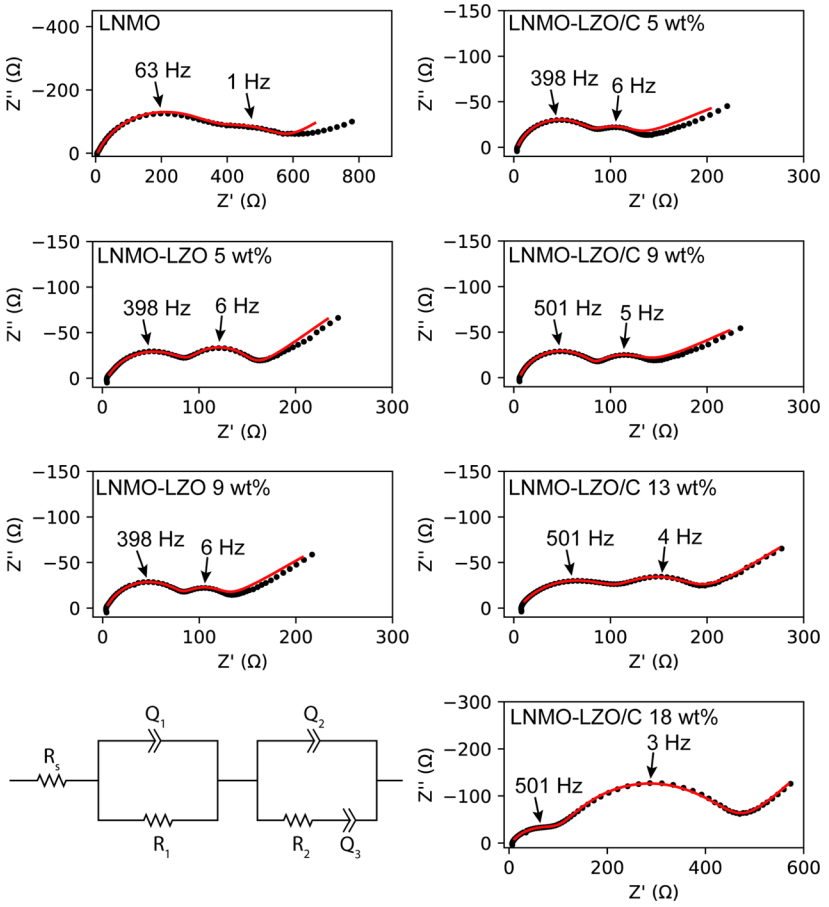

Figure 8. Nyquist plots for the impedance spectra of LNMO, LNMO−LZO/C, and LNMO−LZO half-cells after charging to 4.9 V at 0.2 C with the indicated LZO loadings. The impedance data are represented as black dots, and the red line is the fitted spectrum. The equivalent circuit used to fit the impedance data is also shown.

surface.[38] For the LZO/C cell, the sloping semi-circle could only be fitted with a more complex circuit that included another resistive and capacitive element, likely due to pore resistance (resistance to ion conduction in the electrolyte phase within pores) and double-layer capacitance at an enhanced surface, respectively. Considering the SEM images of the two LZO materials in Figure 2, the more open pore structure of LZO/C and the smaller particle size that results in a greater exposed surface area are likely responsible for these additional spectral features. Bode plots for these samples are shown in Figures S13 and S14.

The average overall resistance (R_1 + R_2) is significantly higher for LZO/C (1230 Ω) than for LZO with battery-grade carbon (330 Ω). This results in a larger overpotential during charging of LNMO−LZO/C cells compared to LNMO−LZO cells, which is observed in the voltage profiles of the corresponding half-cells during the first charging step (Figure 7c). As a consequence, the LZO/C half-cells reach the cut-off potential of 4.9 V versus Li/Li$^+$ at a lower capacity, causing fewer lithium ions to be extracted. This is a limitation of the electrolyte. Greater depths of delithiation would be expected for both LZO and LZO/C with an electrolyte that remains stable at higher potentials.

Blended LNMO−LZO and LNMO−LZO/C half-cells were also studied by impedance spectroscopy to determine if addition of LZO or LZO/C to LNMO had a significant effect on the impedance spectrum after the first charge. A representative impedance spectrum of an LNMO half-cell without a pre-lithiation agent is shown in Figure 8. It features a semi-circle at a higher frequency due to contact and CEI resistance, as well as a semi-circle at a lower frequency corresponding to charge transfer resistance. It is notable that after addition of various amounts of LZO or LZO/C, the general spectral features in the Nyquist plots (Figure 8) and the Bode plots (Figures S15−S21) remain nearly the same, except at high loadings when contributions from contact resistance and possibly pore resistance become very large. Remarkably, in all cases, the pre-lithiated half-cells exhibit a significantly decreased total resistance (R_1 + R_2) compared to cells without any LZO (Table 3).

4. CONCLUSIONS

In this work, we proposed a new Li-rich pre-lithiation additive, LZO, in order to expand the variety of Li-rich pre-lithiation additives available for combinations with different cathode materials. LZO was included as a cathode pre-lithiation additive for an LNMO cathode with a graphite anode in coin-cells. LZO with a sufficient amount of highly conductive Super P carbon was determined to be a better Li$^+$ ion source than LZO/C with intrinsic carbon, releasing 5 Li$^+$ per formula unit of LZO compared to 2−4 Li$^+$ for LZO/C. Among the LZO loading amounts tested, 5 wt % LZO was determined to be optimal, delivering 5 Li$^+$ out of 8 Li$^+$ per formula unit of LZO, corresponding to 550 mA h/g. The LZO additive provided a 10−11% (on the basis of LNMO−LZO mass) or

https://doi.org/10.1021/acsaem.2c02980
ACS Appl. Energy Mater. 2022, 5, 14433−14444

Table 3. Impedance Parameters of Charged LNMO, LNMO–LZO, and LNMO–LZO/C Half-Cells Obtained from Fitting the EIS Spectra and Using the Equivalent Circuit in Figure 8[a]

electrode	n	R_s (Ω)	R_1 (Ω)	R_2 (Ω)	$R_1 + R_2$ (Ω)	Q_1 (μF $s^{\alpha-1}$)	Q_2 (μF $s^{\alpha-1}$)	Q_3 (mF $s^{\alpha-1}$)	α_1	α_2	α_3
LNMO	2	6.6 ± 1.3	370 ± 5	125 ± 80	499	32 ± 1	980 ± 50	29 ± 10	0.75 ± 0.03	0.81 ± 0.09	0.39 ± 0.01
LNMO-LZO-5	3	5.0 ± 0.6	120 ± 48	64 ± 17	184	35 ± 15	310 ± 220	28 ± 10	0.75 ± 0.04	1	0.44 ± 0.05
LNMO–LZO/C-5	2	8.7 ± 7.5	111 ± 38	26 ± 7	136	29 ± 1	340 ± 80	17 ± 4	0.76 ± 0.02	1	0.26 ± 0.01
LNMO–LZO-9	3	7.7 ± 3.2	72 ± 15	41 ± 23	114	45 ± 9	550 ± 40	26 ± 1	0.72 ± 0.02	1	0.38 ± 0.03
LNMO–LZO/C-9	2	5.9 ± 0.1	68 ± 21	45 ± 21	112	27 ± 4	780 ± 350	30 ± 15	0.77 ± 0.01	0.92 ± 0.05	0.33 ± 0.06
LNMO–LZO/C-13	2	5.7 ± 0.8	91 ± 28	85 ± 27	175	64 ± 3	640 ± 150	21 ± 6	0.64 ± 0.04	0.85 ± 0.03	0.39 ± 0.01
LNMO–LZO/C-18	1	4.3	107	344	451	58	320	24	0.61	0.77	0.5

[a]Data is reported as average ± one standard deviation. n is the number of replicate cells used to calculate the average and standard deviation. R_s is the solution resistance. R_1 is the contact resistance between the current collector and the active material and may include CEI resistance. R_2 is a combination of pore resistance and charge transfer resistance of the cathode material. Q_1 is the double-layer capacitance in parallel with the contact resistance. Q_2 is the double-layer capacitance at the cathode material/electrolyte interface. Q_3 is related to mass transport within the cathode material.

15–18% (on the basis of LNMO mass) improvement in reversible capacity and 30% improvement in capacity retention for 50 cycles. This performance was achieved using a process that is compatible with existing cell preparation techniques while keeping the fraction of the additive low and using a more abundant transition metal than cobalt or nickel.[39] Other attractive properties of LZO as a pre-lithiation additive include the low systemic toxicity of oxides of zirconium[40] and the low redox activity of zirconium.

Interestingly, LZO still contains three additional Li^+ per formula unit that can be utilized, in principle, at higher voltages. The incomplete extraction of Li in our cells is mainly attributed to the limitations of the commercial carbonate electrolyte, which does not allow a working potential greater than 5 V versus Li/Li^+.[25] Greater utilization of Li from LZO may be possible in the future with next-generation high-voltage LIBs (Figure S22). The availability of Li-rich pre-lithiation additives operating at a higher voltage, such as LZO, can benefit the development of high-voltage LIBs with higher energy densities since matching the operating potentials of the cathode and the additive is essential.[41]

■ ASSOCIATED CONTENT

Supporting Information

The Supporting Information is available free of charge at https://pubs.acs.org/doi/10.1021/acsaem.2c02980.

Additional voltage profiles, cycle performance comparisons, powder XRD patterns, capacities of full cells, and Nyquist and Bode plots (PDF)

■ AUTHOR INFORMATION

Corresponding Author

Andreas Stein − *Department of Chemistry, University of Minnesota, Minneapolis, Minnesota 55455-0431, United States;* orcid.org/0000-0001-8576-0727; Email: a-stein@umn.edu

Authors

Minog Kim − *Department of Chemistry, University of Minnesota, Minneapolis, Minnesota 55455-0431, United States;* orcid.org/0000-0001-7963-1734

Brian D. Spindler − *Department of Chemistry, University of Minnesota, Minneapolis, Minnesota 55455-0431, United States*

Lifeng Dong − *Department of Physics, Hamline University, Saint Paul, Minnesota 55104, United States;* orcid.org/0000-0002-5536-1319

Complete contact information is available at: https://pubs.acs.org/10.1021/acsaem.2c02980

Author Contributions

A.S. conceived the project. M.K. was responsible for material synthesis, data collection, and analysis. B.D.S. conducted impedance experiments. L.D. provided access to facilities and valuable intellectual feedback. A.S., M.K., and B.D.S. wrote the manuscript. All authors contributed to the discussion and preparation of the manuscript and the Supporting Information.

Notes

The authors declare no competing financial interest.

https://doi.org/10.1021/acsaem.2c02980
ACS Appl. Energy Mater. 2022, 5, 14433−14444

■ ACKNOWLEDGMENTS

This work was partially supported by funding from the Industrial Partnership for Research in Interfacial and Materials Engineering (IPRIME-NMP) at the University of Minnesota. Parts of this work were carried out in the Characterization Facility, University of Minnesota, which receives partial support from the NSF through the MRSEC program. L.D. thanks the Malmstrom Endowed Fund for financial support. The authors would like to thank Professor R. L. Penn for use of the powder X-ray diffractometer, Professor W. H. Smyrl for use of the dry room, and Professor P. Bühlmann for use of the EIS equipment. We also acknowledge Dr. Tran for helpful discussions.

■ REFERENCES

(1) Bruce, P. G.; Freunberger, S. A.; Hardwick, L. J.; Tarascon, J. M. Li−O_2 and Li−S Batteries with High Energy Storage. *Nat. Mater.* **2011**, *11*, 19−29.
(2) Goodenough, J. B.; Park, K. S. The Li-Ion Rechargeable Battery: A Perspective. *J. Am. Chem. Soc.* **2013**, *135*, 1167−1176.
(3) Tarascon, J.-M.; Armand, M. Issues and Challenges Facing Rechargeable Lithium Batteries. *Nature* **2001**, *414*, 359−367.
(4) Julien, C. M.; Mauger, A.; Zaghib, K.; Groult, H. Comparative Issues of Cathode Materials for Li-Ion Batteries. *Inorganics* **2014**, *2*, 132−154.
(5) Zheng, J.; Liang, K.; Shi, K.; Qiu, Y. In Situ Synthesis and Electrochemical Properties of Fe/Li_2O as a High-Capacity Cathode Prelithiation Additive for Lithium Ion Batteries. *Int. J. Electrochem. Sci* **2019**, *14*, 5305−5316.
(6) Sun, Y.; Lee, H. W.; Seh, Z. W.; Liu, N.; Sun, J.; Li, Y.; Cui, Y. High-Capacity Battery Cathode Prelithiation to Offset Initial Lithium Loss. *Nat. Energy* **2016**, *1*, 15008−150014.
(7) Peled, E.; Menkin, S. Review−SEI: Past, Present and Future. *J. Electrochem. Soc.* **2017**, *164*, A1703−A1719.
(8) Holtstiege, F.; Bärmann, P.; Nölle, R.; Winter, M.; Placke, T. Pre-Lithiation Strategies for Rechargeable Energy Storage Technologies: Concepts, Promises and Challenges. *Batteries* **2018**, *4*, 4.
(9) Zou, K.; Deng, W.; Cai, P.; Deng, X.; Wang, B.; Liu, C.; Li, J.; Hou, H.; Zou, G.; Ji, X. Prelithiation/Presodiation Techniques for Advanced Electrochemical Energy Storage Systems: Concepts, Applications, and Perspectives. *Adv. Funct. Mater.* **2021**, *31*, 2005581.
(10) Min, X.; Xu, G.; Xie, B.; Guan, P.; Sun, M.; Cui, G. Challenges of Prelithiation Strategies for Next Generation High Energy Lithium-Ion Batteries. *Energy Storage Mater.* **2022**, *47*, 297−318.
(11) Wang, B. B.; Wang, D.; Li, F.; Wang, J.; Zhou, B. B.; Wang, Y.; Liu, H.; Dou, S. Prelithiation: A Crucial Strategy for Boosting the Practical Application of next-Generation Lithium Ion Battery. *ACS Nano* **2021**, *15*, 2197−2218.
(12) Zhao, J.; Lu, Z.; Liu, N.; Lee, H.-W.; McDowell, M. T.; Cui, Y. Dry-Air-Stable Lithium Silicide-Lithium Oxide Core-Shell Nanoparticles as High-Capacity Prelithiation Reagents. *Nat Commun* **2014**, *5*, 5088.
(13) Zhan, R.; Wang, X.; Chen, Z.; Seh, Z. W.; Wang, L.; Sun, Y. Promises and Challenges of the Practical Implementation of Prelithiation in Lithium-Ion Batteries. *Adv. Energy Mater.* **2021**, *11*, 2101565−2101584.
(14) Diaz-Lopez, M.; Chater, P. A.; Bordet, P.; Freire, M.; Jordy, C.; Lebedev, O. I.; Pralong, V. Li_2O:Li−Mn−O Disordered Rock-Salt Nanocomposites as Cathode Prelithiation Additives for High-Energy Density Li-Ion Batteries. *Adv. Energy Mater.* **2020**, *10*, 1902788.
(15) Sun, Y.; Lee, H. W.; Zheng, G.; Seh, Z. W.; Sun, J.; Li, Y.; Cui, Y. In Situ Chemical Synthesis of Lithium Fluoride/Metal Nanocomposite for High Capacity Prelithiation of Cathodes. *Nano Lett.* **2016**, *16*, 1497−1501.
(16) Kim, M. G.; Cho, J. Air Stable Al_2O_3-Coated Li_2NiO_2 Cathode Additive as a Surplus Current Consumer in a Li-Ion Cell. *J. Mater. Chem.* **2008**, *18*, 5880−5887.
(17) Su, X.; Lin, C.; Wang, X.; Maroni, V. A.; Ren, Y.; Johnson, C. S.; Lu, W. A New Strategy to Mitigate the Initial Capacity Loss of Lithium Ion Batteries. *J. Power Sources* **2016**, *324*, 150−157.
(18) Zhang, L.; Dose, W. M.; Vu, A. D.; Johnson, C. S.; Lu, W. Mitigating the Initial Capacity Loss and Improving the Cycling Stability of Silicon Monoxide Using Li_5FeO_4. *J. Power Sources* **2018**, *400*, 549−555.
(19) Noh, M.; Cho, J. Role of Li_6CoO_4 Cathode Additive in Li-Ion Cells Containing Low Coulombic Efficiency Anode Material. *J. Electrochem. Soc.* **2012**, *159*, A1329−A1334.
(20) Arora, P.; White, R. E.; Doyle, M. Capacity Fade Mechanisms and Side Reactions in Lithium-Ion Batteries. *J. Electrochem. Soc.* **1998**, *145*, 3647−3667.
(21) Johnson, C. S.; Kang, S. H.; Vaughey, J. T.; Pol, S. V.; Balasubramanian, M.; Thackeray, M. M. Li_2O Removal from Li_5FeO_4: A Cathode Precursor for Lithium-Ion Batteries. *Chem. Mater.* **2010**, *22*, 1263−1270.
(22) Huang, S.; Wilson, B. E.; Wang, B.; Fang, Y.; Buffington, K.; Stein, A.; Truhlar, D. G. Y-doped Li_8ZrO_6: A Li-Ion Battery Cathode Material with High Capacity. *J. Am. Chem. Soc.* **2015**, *137*, 10992−11003.
(23) Huang, S.; Wilson, B. E.; Smyrl, W. H.; Truhlar, D. G.; Stein, A. Transition-Metal-Doped M-Li_8ZrO_6 (M = Mn, Fe, Co, Ni, Cu, Ce) as High- Specific-Capacity Li-Ion Battery Cathode Materials: Synthesis, Electrochemistry, and Quantum Mechanical Characterization. *Chem. Mater.* **2016**, *28*, 746−755.
(24) Huang, S.; Fang, Y.; Wang, B.; Wilson, B. E.; Tran, N.; Truhlar, D. G.; Stein, A. Conduction and Surface Effects in Cathode Materials: Li_8ZrO_6 and Doped Li_8ZrO_6. *J. Phys. Chem. C* **2016**, *120*, 9637−9649.
(25) Tran, N.; Spindler, B. D.; Yakovenko, A. A.; Wiaderek, K. M.; Chapman, K. W.; Huang, S.; Smyrl, W. H.; Truhlar, D. G.; Stein, A. Effective Electrochemical Charge Storage in the High-Lithium Compound Li_8ZrO_6. *ACS Appl. Energy Mater.* **2019**, *2*, 1274−1287.
(26) Betz, J.; Nowak, L.; Winter, M.; Placke, T.; Schmuch, R. An Approach for Pre-Lithiation of $Li_{1+x}Ni_{0.5}Mn_{1.5}O_4$ Cathodes Mitigating Active Lithium Loss. *J. Electrochem. Soc.* **2019**, *166*, A3531−A3538.
(27) Gabrielli, G.; Marinaro, M.; Mancini, M.; Axmann, P.; Wohlfahrt-Mehrens, M. A New Approach for Compensating the Irreversible Capacity Loss of High-Energy Si/C|$LiNi_{0.5}Mn_{1.5}O_4$ Lithium-Ion Batteries. *J. Power Sources* **2017**, *351*, 35−44.
(28) Mancini, M.; Axmann, P.; Gabrielli, G.; Kinyanjui, M.; Kaiser, U.; Wohlfahrt-Mehrens, M. A High-Voltage and High-Capacity $Li_{1+x}Ni_{0.5}Mn_{1.5}O_4$ Cathode Material: From Synthesis to Full Lithium-Ion Cells. *ChemSusChem* **2016**, *9*, 1843−1849.
(29) Dose, W. M.; Blauwkamp, J.; Piernas-Muñoz, M. J.; Bloom, I.; Rui, X.; Klie, R. F.; Senguttuvan, P.; Johnson, C. S. Liquid Ammonia Chemical Lithiation: An Approach for High-Energy and High-Voltage Si-Graphite|$Li_{1+x}Ni_{0.5}Mn_{1.5}O_4$ Li-Ion Batteries. *ACS Appl. Energy Mater.* **2019**, *2*, 5019−5028.
(30) Chen, Y.; Li, Y.; Tang, S.; Guo, J.; Lei, T.; Deng, S.; Chang, S.; Zhu, J. Synthesis of $LiNi_{0.5}Mn_{1.5}O_4$ via Ammonia-Free Co-Precipitation Method: Insight in the Effects of the Lithium Additions on the Morphology, Structure and Electrochemical Properties. *ChemistrySelect* **2019**, *4*, 393−398.
(31) Yin, X. S.; Zhang, Q. H.; Yu, J. G. Three-Step Calcination Synthesis of High-Purity Li_8ZrO_6 with CO_2 Absorption Properties. *Inorg. Chem.* **2011**, *50*, 2844−2850.
(32) Barnakov, C. N.; Khokhlova, G. P.; Popova, A. N.; Romanenko, A. I.; Bryantsev, Y. A. Structure and Conductivity of Carbon Materials Produced from Coal Pitch with Carbon Additives. *Coke Chem.* **2017**, *60*, 278−284.
(33) Wang, J.; Yamada, Y.; Sodeyama, K.; Chiang, C. H.; Tateyama, Y.; Yamada, A. Superconcentrated Electrolytes for a High-Voltage Lithium-Ion Battery. *Nat. Commun.* **2016**, *7*, 12032−12040.
(34) Arrebola, J. C.; Caballero, A.; Cruz, M.; Hernán, L.; Morales, J.; Castellón, E. R. Crystallinity Control of a Nanostructured $LiNi_{0.5}Mn_{1.5}O_4$ Spinel via Polymer-Assisted Synthesis: A Method for Improving Its Rate Capability and Performance in 5 V Lithium Batteries. *Adv. Funct. Mater.* **2006**, *16*, 1904−1912.

https://doi.org/10.1021/acsaem.2c02980
ACS Appl. Energy Mater. 2022, 5, 14433−14444

(35) Park, K. S.; Im, D.; Benayad, A.; Dylla, A.; Stevenson, K. J.; Goodenough, J. B. $LiFeO_2$-Incorporated Li_2MoO_3 as a Cathode Additive for Lithium-Ion Battery Safety. *Chem. Mater.* **2012**, *24*, 2673−2683.
(36) An, S. J.; Li, J.; Daniel, C.; Mohanty, D.; Nagpure, S.; Wood, D. L. The State of Understanding of the Lithium-Ion-Battery Graphite Solid Electrolyte Interphase (SEI) and Its Relationship to Formation Cycling. *Carbon* **2016**, *105*, 52−76.
(37) Kasnatscheew, J.; Evertz, M.; Streipert, B.; Wagner, R.; Klöpsch, R.; Vortmann, B.; Hahn, H.; Nowak, S.; Amereller, M.; Gentschev, A. C.; Lamp, P.; Winter, M. The Truth about the 1st Cycle Coulombic Efficiency of $LiNi_{1/3}Co_{1/3}Mn_{1/3}O_2$ (NCM) Cathodes. *Phys. Chem. Chem. Phys.* **2016**, *18*, 3956−3965.
(38) Pritzl, D.; Bumberger, A. E.; Wetjen, M.; Landesfeind, J.; Solchenbach, S.; Gasteiger, H. A. Identifying Contact Resistances in High-Voltage Cathodes by Impedance Spectroscopy. *J. Electrochem. Soc.* **2019**, *166*, A582−A590.
(39) Abundance of Elements in the Earth's Crust and in the Sea. In *Handbook of Chemistry and Physics*, 100th ed.; Rumble, J. R., Ed.; CRC Press, 2019; p 14-18.
(40) Couture, P.; Blaise, C.; Cluis, D.; Bastien, C. Zirconium Toxicity Assessment Using Bacteria, Algae and Fish Assays. *Water Air Soil Pollut.* **1989**, *47*, 87−100.
(41) Wu, F.; Maier, J.; Yu, Y. Guidelines and Trends for Next-Generation Rechargeable Lithium and Lithium-Ion Batteries. *Chem. Soc. Rev.* **2020**, *49*, 1569−1614.

https://doi.org/10.1021/acsaem.2c02980
ACS Appl. Energy Mater. 2022, 5, 14433−14444